Nanoscale

PAPER

View Article Online
View Journal | View Issue

Cite this: *Nanoscale*, 2014, **6**, 6798

A hydride-induced-reduction strategy for fabricating palladium-based core–shell bimetallic nanocrystals†

Xingli Wang, Binghui Wu, Guangxu Chen, Yun Zhao, Pengxin Liu, Yan Dai and Nanfeng Zheng*

Received 17th January 2014
Accepted 15th March 2014

DOI: 10.1039/c4nr00302k

www.rsc.org/nanoscale

One key challenge in making high-quality bimetallic nanocrystals is to prevent self-nucleation of individual metal components. We report in this work an effective seeded growth strategy that uses activated hydrogen atoms as the reducing agent to prepare core–shell bimetallic nanocrystals. In the developed method, Pd nanocrystals serve as the seed and catalyst as well to activate H_2 for the reductive deposition of Ag. The unique feature of the developed method is that the activated hydrogen atoms are confined on the surface of the Pd seeds. Consequently, the self-nucleation of Ag is effectively inhibited so that the deposition of Ag occurs only on Pd. The mechanism studies reveal that reductive growth of Ag on Pd seeds proceeds until the Pd surface is fully covered by Ag. The Ag/Pd ratio in the prepared Pd@Ag nanocrystals is readily fine-tuned by the amount of $AgNO_3$ or H_2. The method is effective for depositing Ag on Pd nanocrystal seeds with different morphologies such as nanosheets, nanocubes, tetrahedra and nanowires. More importantly, the deposition of Ag on Pd nanowires allows preparation of flexible transparent electrode material with sheet electronic conductivity of 271 S sq^{-1} at a transmittance of over 90%.

1 Introduction

Bimetallic nanocrystals (NCs) containing noble metals, such as Au, Ag, Pd, Pt and Rh, have received intensive research interest in the past decades.[1–6] The integration of noble metals with transition metals in bimetallic nanocrystals often creates synergetic effects induced by tuning the electronic structure due to charge transfer or structural strain between metals, interfacial collaboration by two metals, and interfacial stabilization. In many cases, such synergetic effects endow noble metal-based bimetallic nanocrystals with unique optical, catalytic, and magnetic properties which are distinctly different from those of their monometallic counterparts.[7] A number of methods have been developed to synthesize bimetallic NCs. The developed methods include co-reduction of metal salts,[8] galvanic replacement reaction,[9,10] thermal deposition of organometallic compounds,[11,12] seed-mediated growth and so on. Among the developed synthetic methods, seed-mediated growth has been well-documented as an effective route to synthesize core@shell and heterostructured bimetallic NCs.[13,14] In a typical seed-mediated growth method, the pre-made seeds of one metal serve as nucleation sites for further growth of the secondary metal. The resulting structure depends highly on how the secondary metals deposit on the surface of the seeds.[15] Kinetic factors play important roles during subsequent reductive growth of the secondary metals. A too fast reduction rate caused by a strong reducing agent often breaks the near equilibrium condition, resulting in separate nucleation of the secondary metals and thus preventing formation of high-quality bimetallic nanocrystals.

To prevent self-nucleation of secondary metals, their reduction needs to be confined on the surface of seeded nanocrystals. Recently, Li and co-workers have developed an effective system to prepare Au–Co core–shell NCs, Au–Ni spindly nanostructures and Au–Cu alloy by using octadecylamine (ODA) as both the solvent and the surfactant.[16] At the reaction temperature, reduction of non-noble metal ions by ODA only took place with the help of the preformed Au nanocrystal seeds. Such so-called "noble-metal-induced-reduction (NMIR) strategy" nicely confined the reductive growth of non-noble metals on the preformed nanocrystal seeds. The size and morphology of the resulting products could thus be controlled by the concentration of precursors and the reaction temperature. In this strategy, the presence of a high-excess amount of potential reducing agent (*i.e.*, ODA) required delicate control over the reaction thermodynamics to prevent self-nucleation of the

State Key Laboratory for Physical Chemistry of Solid Surfaces, Collaborative Innovation Center of Chemistry for Energy Materials and Department of Chemistry, College of Chemistry and Chemical Engineering, Xiamen University, Xiamen 361005, China. E-mail: nfzheng@xmu.edu.cn; Web: http://chem.xmu.edu.cn/groupweb/nfzheng/index.asp

† Electronic supplementary information (ESI) available. See DOI: 10.1039/c4nr00302k

secondary metals, particularly when the secondary metals (*i.e.*, Ag) are rather easily reduced.

By utilizing the property that H_2 can be easily split and activated on the Pd surface into highly active H atoms, we now report an effective strategy to synthesize Pd-based bimetallic NCs by using Pd nanocrystals as seeds and activated hydrogen atoms as the reducing agent. Pd is an excellent hydrogen-storage material owing to its prominent properties to split molecular hydrogen atoms into H atoms and include them in their lattice and surface as well.[17,18] The activated H atoms can serve as a much stronger reducing agent than molecular hydrogen.[19,20] Although the reduction of Ag^+ cannot occur in the presence of molecular H_2 at room temperature, the activated H species on Pd are readily reduced Ag^+ to yield metallic Ag. Since the activated hydrogen species are nicely confined on the surface of Pd, the reduction of Ag^+ takes place only on Pd. In such autocatalytic reduction process, self-nucleation of Ag can be effectively avoided. In this work, we first used Pd nanosheets for the demonstration of the concept since the coating process of Ag on these Pd nanosheets is readily monitored by optical means.[2] Detailed studies revealed that the reductive growth of Ag on Pd nanosheets proceeded until the Pd surface was fully covered by Ag. The catalytic reduction of Ag on Pd was not morphology-dependent. The surface-confined reduction mechanism was therefore successfully applied to prepare core–shell Pd@Ag nanocubes, tetrahedra and nanowires. In the case of Pd nanowires, the developed facile Ag deposition method helped fabricate flexible transparent conductive films.

2 Experimental

2.1 Chemicals and materials

Palladium(II) acetylacetonate [$Pd(acac)_2$] (99%) was purchased from Alfa Aesar. Poly(vinylpyrrolidone) (PVP, $M_W = 58\,000$, AR), tetrabutylammonium bromide (TBAB), palladium(II) chloride ($PdCl_2$), silver nitrate ($AgNO_3$), sodium iodide (NaI), and *N*,*N*-dimethylformamide (DMF) were purchased from Sinopharm Chemical Reagent Co. Ltd. (Shanghai, China). Hydrogen gas (99.99%). All reagents were used as received without further purification.

2.2 Synthesis of Pd nanosheets

Pd nanosheets were obtained according to our previous work with further modification.[21] 50 mg $Pd(acac)_2$, 160 mg PVP and 160 mg TBAB were dissolved in 10 mL DMF. Then 2 mL water was added into the as-prepared solution. The resulting homogeneous solution was transferred to a glass pressure vessel. After being charged with CO to 1 bar, the vessel was heated from room temperature to 60 °C in 30 min and kept at this temperature for 150 min with stirring. As the reaction progressed, the colour of the reaction mixture changed from yellow to light blue, and finally to dark blue. The resulting blue colloidal products were collected by centrifugation, and washed several times with ethanol and acetone.

2.3 Synthesis of Pd nanocubes

50 mg $Pd(acac)_2$ and 160 mg PVP were dissolved in 10 mL DMF. 300 mg NaI was dissolved in 2 mL water and then added into the as-prepared solution. The resulting homogeneous dark red solution was transferred to a Teflon-lined stainless-steel autoclave with a capacity of 20 mL. The sealed vessel was then heated from room temperature to 150 °C in 20 min and stayed at 150 °C for 8 h before it was cooled down to room temperature. The products were precipitated by acetone, separated *via* centrifugation at 8000 rpm and further purified twice by ethanol and acetone.[22]

2.4 Synthesis of Pd tetrapod nanocrystals

10 mg of $Pd(acac)_2$, 90 mg of PVP were dissolved in 10 mL DMF. The resulting homogeneous solution was transferred to a glass pressure vessel. After being charged with $CO : H_2 = 1 : 4$ to 2 bar, the vessel was heated from room temperature to 100 °C in 20 min and kept at this temperature for another 160 min with stirring. The resulting products were collected by centrifugation and washed several times with ethanol and acetone.[23]

2.5 Synthesis of Pd nanowires

Pd nanowires were synthesized according to our previous work with further modification.[24] 17.7 mg $PdCl_2$, 300 mg NaI and 800 mg PVP were dissolved in 10 mL water. The resulting solution was stirred overnight at room temperature and then transferred to a Teflon-lined stainless-steel autoclave with a capacity of 20 mL. The sealed vessel was then heated from room temperature to 200 °C in 90 min and stood at 200 °C for 2 h before it was cooled to room temperature. The products were precipitated by isopropanol, separated *via* centrifugation at 8000 rpm and further purified twice by an ethanol–isopropanol mixture. After the final centrifugation, the precipitate of Pd NWs was dispersed in ethanol. It is noticeable that the wire solution is less concentrated. This is because this wire recipe generates numerous big palladium particles, which are removed during centrifugation.

2.6 Synthesis of Pd@Ag nanostructures with different amounts of $AgNO_3$

Different shapes of Pd seeds (*i.e.*, nanocubes, tetrapods, and five-fold twinned nanowires) were employed as seeds and dispersed in 5 mL water in a 25 mL two-necked flask. H_2 gas was continuously bubbled though the solution for 40 min at room temperature. Then the H_2 gas was moved away and the system remained to be closed. 1 mL $AgNO_3$ solution was injected by an injector under stirring. The ratio of H_2/Pd was varying from 0.5, 1, 2, 5 and 10. After 1 h, the reaction was stopped by venting the system. The products were collected *via* centrifugation at 14500 rpm.

2.7 Synthesis of Pd@Ag nanosheets with different amounts of H_2

Pd nanosheets were used as seeds and dispersed in 3 mL water in a 5 mL flask. Then 10-time-molar $AgNO_3$ compared to that of

Pd was added into the resulting solution. A gas-tight syringe was employed to inject different amounts of H_2 in this closed system. The ratio of H/Pd was varied from 1, 2, 5 and 10. After 12 h, the system was opened. The products were collected *via* centrifugation at 14500 rpm.

2.8 Fabrication of Pd-based transparent conductive film

The Pd ink was prepared as follows: the as-made Pd nanowires were washed several times, then dispersed in ethanol and sonicated for 30–60 s. 50 μL of the Pd ink (2.4 mg mL^{-1}) was consequently deposited on a 140 μm-thick polyethylene terephthalate (PET) substrate by spin coating technique. The obtained Pd film was dried under an infrared lamp. After drying, the film was transferred in a tube furnace and heated at 130 °C in 5% H_2/N_2 to anneal the Pd nanowires. The Pd nanowires film (denoted as Pd NWs film) was treated with aqueous Ag^+ solution in the presence of H_2 at room temperature to allow the deposition of Ag on their surfaces (denoted as Pd NWs film@Ag). For comparison, pre-prepared Pd@Ag nanowires were also employed as the materials to fabricate the film (denoted as Pd@Ag NWs film) by depositing them on PET *via* spinning coating.

2.9 Characterizations

TEM (including high-resolution transmission electron microscope, HRTEM) studies were performed on a TECNAI F-30 high-resolution transmission electron microscope operating at 300 kV. The samples were prepared by dropping ethanol dispersion of samples onto 300-mesh carbon-coated copper grids and immediately evaporating the solvent. SEM images were taken on an HICATHI S-4800 Sirion SEM. The percentages of Pd and Ag in the samples were determined using inductively coupled plasma spectrometry (ICP). The samples for ICP were prepared by dissolving equal Pd@Ag bimetallic NCs with HNO_3 or aqua-regia to detect Ag ions or Pd ions, respectively. The absorption spectra were obtained from a UV-Vis-NIR spectrophotometer (Varian, Cary5000). The electrochemical measurements of the catalysts were performed using an electrochemical work station (CHI760D).

2.10 Electrochemical measurements

Ethanol dispersion of purified nanoparticles was deposited on a glassy carbon electrode to obtain the working electrodes after the solvent was dried by an IR lamp. A saturated calomel electrode (SCE) and a platinum foil were used as the reference and counter electrode, respectively. The cyclic voltammograms were recorded at a sweep rate of 50 mV s^{-1} in 0.5 M H_2SO_4. Before cyclic voltammetry (CV) measurements, the electrolyte was purged with high purity N_2 gas for at least 30 min to ensure the gas saturated.

2.11 Sheet resistance measurement

Pd-based transparent conductive films resistance measurements were made using the four-probe technique with silver paste electrodes of dimensions and spacings of typically 10 mL in size and a Keithley 2400 source meter.

3 Results and discussion

To demonstrate the capability of metal surface-activated hydrogen for inducing the reduction of alternative metal ions, a system using Pd nanosheets to promote the reduction of Ag^+ at room temperature was first chosen for the following two reasons: (1) at room temperature, Ag^+ cannot be chemically reduced by H_2 and (2) the deposition of Ag on Pd nanosheets yielded Pd@Ag core–shell nanosheets displaying different UV-Vis absorption spectra from Pd nanosheets, making it possible to spectroscopically monitor the deposition process. The hexagonal Pd nanosheets used in the studies had a thickness of 1.8 nm and an average mean diameter (diagonal of the hexagon) of 50 nm (Fig. S1†). In the absence of Pd, the aqueous solution of $AgNO_3$ remained transparent and colorless after bubbling with H_2 although a small amount of $NaBH_4$ immediately turned the Ag^+ solution into dark yellow (Fig. S2†). This result clearly illustrated that H_2 alone couldn't reduce Ag^+ to Ag(0) at room temperature. However, when Pd nanosheets were introduced into the Ag^+ aqueous solution, H_2 readily induced the reduction of Ag^+ at room temperature. As shown in Fig. 1, when the light blue solution of Pd nanosheets were first treated by H_2 bubbling, the introduction of Ag^+ rapidly changed the color of the solution into brown. Further addition of Ag^+ continued to change the color of the solution. As monitored by UV-Vis spectroscopy, the maximum optical absorption of the resulted solution changed from 1087 to 1044, 990, 911, and 870 nm when the $AgNO_3$/Pd ratio was increased from 0 to 0.5, 1, 2 and 5,

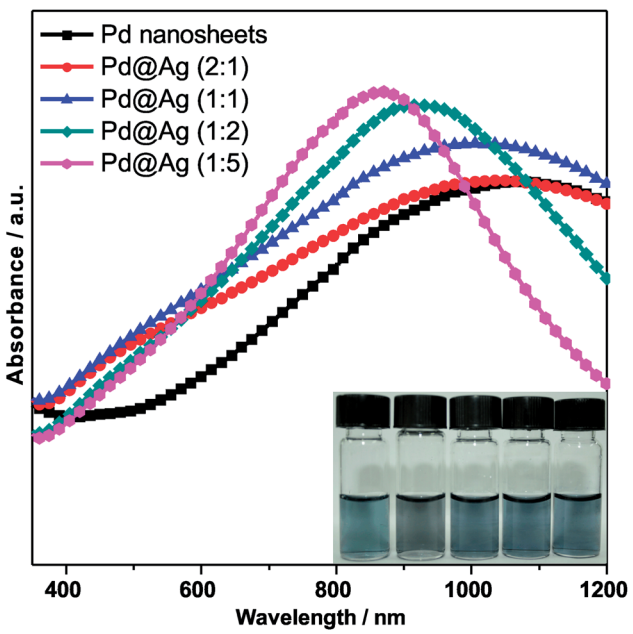

Fig. 1 UV-Vis absorption spectra and digital photographs (inset) of the Pd@Ag core–shell bimetallic nanosheets prepared by varying the $AgNO_3$/Pd molar ratio. From left to right, the samples in the inset were prepared using $AgNO_3$/Pd ratios of 0.5, 1, 2 and 5, respectively.

respectively. Such a blue-shift of the absorption spectra was caused by the aspect ratio (the diameter-to-thickness ratio) of the obtained Pd@Ag nanosheets, clearly indicating successful deposition of Ag on the H_2-treated Pd nanosheets.

Transmission electron microscopy (TEM) was employed to further investigate the overgrowth structure of Ag on Pd nanosheets. As illustrated in Fig. 2, the obtained Pd@Ag nanosheets with $AgNO_3$/Pd supplied in 1 : 1 were roughly shaped in hexagons. The mean diameter of Pd@Ag nanosheets was maintained at ~50 nm. The large-area TEM image and STEM image (Fig. S3†) revealed that no isolated Ag nanoparticles caused by self-nucleation were present in the products. The high-resolution TEM (HRTEM) image (Fig. 2d) of the Pd@Ag nanosheets showed well-defined lattice fringes with an interplanar spacing of 0.23 nm, corresponding to {111} planes of face-center-cubic Ag. Moreover, both the energy-dispersive X-ray (EDX) line profile (Fig. 2e) and the elemental-mapping analysis (Fig. 2f) revealed that Ag and Pd atoms were homogeneously distributed throughout the as-prepared core@shell Pd@Ag nanosheets, suggesting that the growth of Ag was confined on the Pd surface. It is worth mentioning that the Pd@Ag nanosheets were not flat and perfect hexagons any more. Some crimpy feature was clearly observed. Such a structural change further indicated that the deposition of Ag on the Pd nanosheets was closely related to the Pd hydride formation in the system.[25] The lattice expansion of Pd nanosheets induced by the H insertion followed by the subsequent lattice contraction caused by the H releasing during Ag^+ reduction process would be the main reason for the structure change.[25]

Upon bubbling with H_2, Pd nanosheets were converted into Pd hydride, PdH_x. Each H atom in PdH_x is expected to donate one electron to reduce one Ag^+ ion. Since x in all forms of Pd hydride is not larger than 1, the molar amount of deposited Ag should not be larger than that of Pd. However, our experiments clearly demonstrated that the ratio of the deposited amount of Ag to Pd could be higher than 1. Pd@Ag nanosheets with different Ag/Pd ratios were readily prepared by varying the concentrations of Ag^+ introduced in the system. As revealed by TEM measurements, the thickness of the obtained Pd@Ag nanosheets increased as the Ag/Pd ratio increased in the system although the core–shell nanosheets had almost the same diameter as the parental Pd nanosheets. The thickness of the obtained Pd@Ag nanosheets was increased from 2.9 to 6.0 nm as the $AgNO_3$/Pd molar ratio was increased from 1 to 10 (Fig. S4 and S5†). The actual composition of the Pd@Ag nanosheets was determined by ICP analysis (Table S1†). The ratio of Ag to Pd in the obtained Pd@Ag nanosheets was increased from 0.3 to 4.2 when the Ag/Pd initial ratio in the system was increased from 0.5 to 5. More importantly, the value of Ag/Pd ratio was kept at 4.2, but not further increased even when the Ag/Pd ratio was continued to increase to 10. These results suggested that (1) the hydrogen involved in the reduction process was not limited to the hydrogen confined in the Pd nanosheets and (2) the deposition of Ag was self-limited.

On the basis of the above results, the overgrowth mechanism of Ag on Pd in the presence of H_2 was proposed. In the proposed mechanism (Fig. 3), the hydrogen atoms confined in the Pd nanosheets are the active agents to reduce Ag^+ to Ag(0) which is then directly deposited on Pd while the hydrogen atoms are converted into H^+. The deposition of Ag can continue to occur until no more H_2 can be absorbed and activated on Pd. At room temperature, the palladium hydride phase diagram consists of α phase with low hydrogen content, β phase with high hydrogen content, and an intermediate miscibility gap consisting of both α and β phases.[26–28] Our previous studies also revealed that β-PdH_x existed in freshly obtained Pd tetrapod nanocrystals and then were gradually transformed into pure Pd nanocrystals in air.[23] It is therefore reasonable to consider palladium hydride as the active agent to reduce Ag^+. As expected, the reductive deposition of Ag^+ on Pd led to the production of H^+ and thus decreased of pH values of the solutions. The pH value of Pd@Ag (1 : 1) was almost the same as the theoretical value obtained by assuming the reduction of Ag^+ gave the same moles of H^+. When more Ag^+ was reduced, the pH value decreased more (Table S2†).

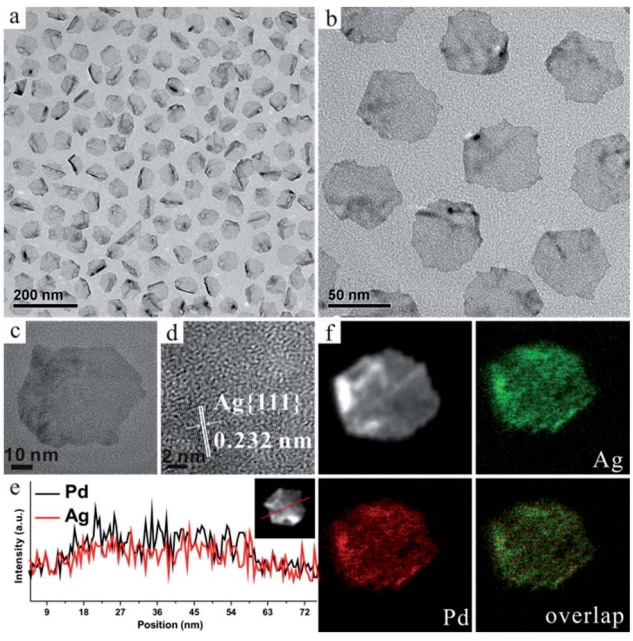

Fig. 2 (a–c) Representative TEM images of Pd@Ag (1 : 1) core–shell bimetallic nanosheets. (d) HRTEM, (e) HAADF-STEM image and EDX line profiles, (f) EDX mapping images of an individual Pd@Ag (1 : 1) nanosheet.

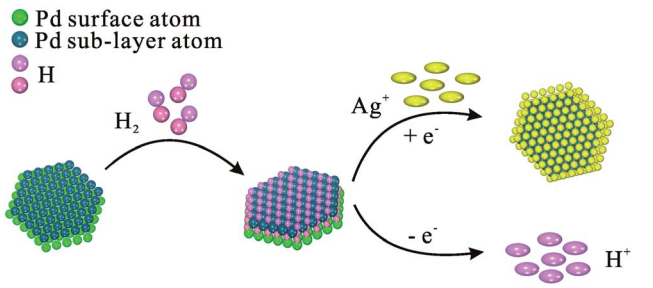

Fig. 3 Proposed reaction mechanism for the synthesis of Pd@Ag core–shell nanocrystals in the presence of H_2.

Once transferred from hydrogen atoms, the electrons can move around in the metallic Pd@Ag nanosheets. As a result, the reductive deposition of Ag^+ on Pd does not need to take place at the locations of activated hydrogen. Such situation helps to explain why the Ag/Pd ratio in the obtained Pd@Ag nanosheets could be higher than 1. When carefully considered, the hydrogen in the reaction system essentially consisted of three parts: (1) hydrogen confined in Pd nanosheets as hydride; (2) the dissolved hydrogen in water and (3) gaseous hydrogen remaining in the reaction vessel. As soon as there are surface-exposed Pd atoms, gaseous hydrogen can continue to be absorbed and activated onto Pd@Ag nanosheets for reductive deposition of Ag on the nanosheets. When Pd atoms are fully covered by Ag atoms and thus no more H_2 can be activated, the deposition of Ag stops. In a certain potential region, the adsorption/desorption of hydrogen occurs easily on surface-exposed Pd. In our studies, the exposure of Pd was thus determined by cyclic voltammetry (CV) to directly correlate the termination of Ag deposition process with the lack of surface-exposed Pd atoms. As shown in Fig. 4, when the Ag/Pd ratio used was 0.5, the obtained Pd@Ag nanosheets were still active for the hydrogen adsorption/desorption in the potential region between −0.2 and 0.1 V, indicating the exposure of Pd atoms on their surface. When the Ag/Pd ratio was increased to 1, the current densities in the hydrogen adsorption/desorption region became much smaller. When the Ag/Pd initial ratio continued to increase to 5, no current was observed in the hydrogen adsorption/desorption region any more, indicating that Pd was fully covered by Ag. This result well explains why further increase of Ag^+/Pd did not increase the ratio of Ag/Pd in the obtained core–shell Pd@Ag nanosheets, and further supports the proposed overgrowth mechanism.

In the cases when the supplied hydrogen was highly in excess, the Ag/Pd ratio in the obtained Pd@Ag nanosheets was readily controlled by the Ag/Pd ratio provided in the synthesis until Pd was fully covered. According to the proposed deposition mechanism, we also found it possible to adjust the Ag/Pd ratio and thus the thickness of Pd@Ag nanosheets by varying the amount of H_2 in the system. In our studies, a gas-tight syringe was employed to inject different amounts of H_2 into a closed 5 mL flask containing 3 mL aqueous solution of Pd nanosheets and $AgNO_3$ with an initial Ag/Pd molar ratio of 10. The ratio of H/$AgNO_3$ was varied from 1, 2, 5 and 10. As illustrated in Fig. 5, uniform Pd@Ag nanosheets were also successfully prepared. The as-prepared Pd@Ag nanosheets were flat in all ratios mainly because of the injected H_2 interacting with the Pd surface slowly. The EDX analysis indicated that all the products contained both Ag and Pd element. The actual composition of the Pd@Ag nanosheets was further analysed by ICP. As shown in Table S3,† the ratio of Ag to Pd in the obtained Pd@Ag nanosheets was 0.86 to 1 when the H/Pd ratio was 1. The value increased from 0.86 to 4.25 when the injected hydrogen in the system was gradually increased. The amounts of Ag in different Pd@Ag samples were perfectly consistent with that of the introduced H_2, indicating the validity of this method. However, as observed in the CV curves of the Pd@Ag nanoparticles, when the ratio of Ag to Pd reached *ca.* 4, the surface of Pd nanosheets was fully covered, hindering further deposition of Ag^+ on Pd nanosheets.

To further demonstrate the generality of the Pd–H assisted deposition strategy discussed above, well-defined Pd nanostructures other than nanosheets (*i.e.*, nanocubes, tetrapods, and five-fold twinned nanowires) were also prepared and used as the seeds for the deposition of alternative metals. As illustrated in Fig. 6a and b, the introduction of H_2 allowed facile deposition of Ag on Pd nanocubes and Pd tetrapods. In the presence of H_2, mixing Ag^+ with Pd nanocubes (diameter of 13.8 nm) in a Ag^+/Pd ratio of 1 : 1 produced uniform core–shell Pd@Ag particles with an increased average diameter of 15.5 nm. The Ag overlayer completely covered the cubic seeds (Fig. S6†).

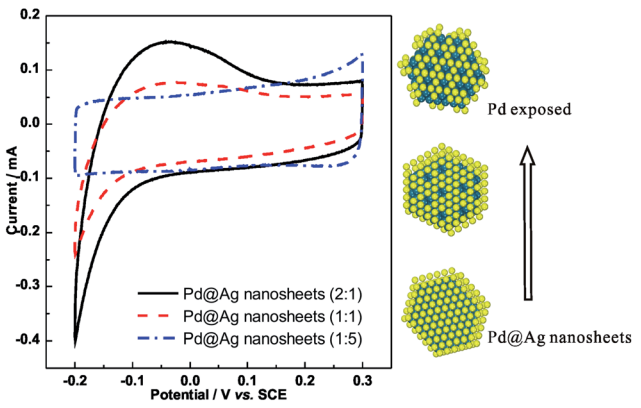

Fig. 4 CV curves of the Pd@Ag nanosheets with $AgNO_3$/Pd ratios of 0.5, 1 and 5, respectively.

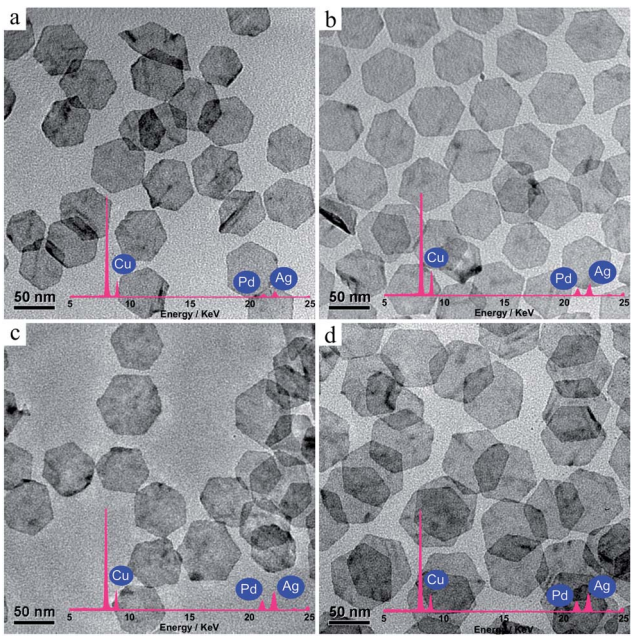

Fig. 5 TEM images of the Pd@Ag nanosheets in different molar ratios. H/Pd ratios of (a) 1, (b) 2, (c) 5, and (d) 10, respectively. (Inset: EDX analysis of the as-prepared Pd@Ag nanosheets.)

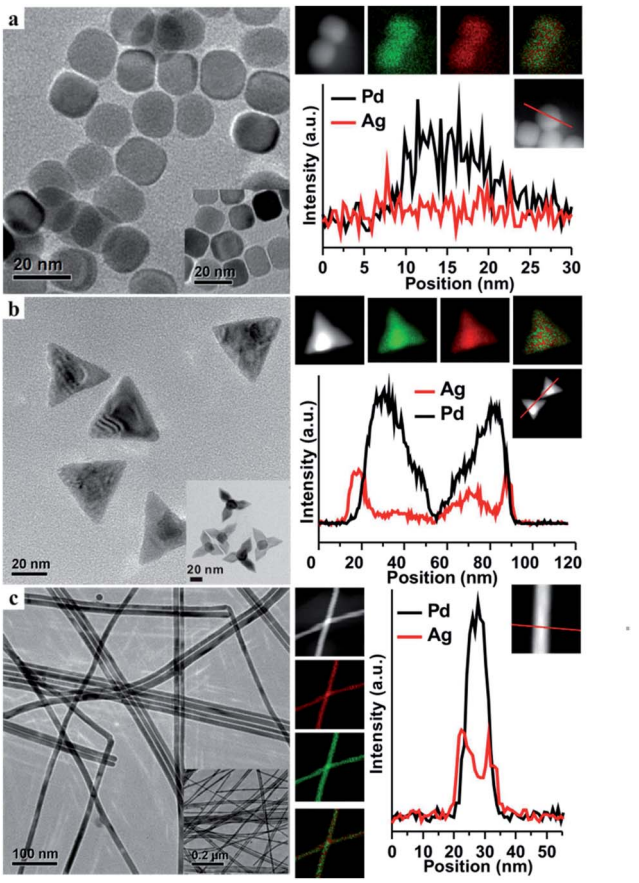

Fig. 6 Representative TEM images, EDX mapping images, HAADF-STEM image and EDX line profiles of K edges of Pd and Ag in (a) Pd cube@Ag (1 : 1), (b) Pd tetrapod@Ag (1 : 1), and (c) Pd wire@Ag (1 : 1). Insets are the corresponding seeds (*i.e.*, Pd cubes, Pd tetrapods, Pd nanowires). EDX mapping images: red represents Pd and green Ag.

When the amount of Ag^+ was increased to 10 times of Pd, the side-length of Pd@Ag further increased to 16.8 nm (Table S4†). In the case of Pd tetrapods which are enclosed by {111} surfaces, preferential deposition of Ag on the concave surfaces of the tetrapods was clearly revealed even when Ag^+ was supplied in the 1 : 1 molar ratio to Pd (Fig. 6b). When the $AgNO_3$/Pd ratio was increased to 10, the deposition of Ag on Pd tetrapods eventually produced Pd@Ag tetrahedrons without the presence of noticeable concave surfaces (Fig. S7†).

Two-dimensional metal nanowires are attractive materials for fabrication transparent conductive electrodes for various applications such as organic light-emitting diodes and solar cells.[29–33] Although the synthesis of Pd nanowires has been achieved in the literature, no attempts have been reported to use Pd nanowires made by wet-chemistry to fabricate electrically conductive films. In this study, we have demonstrated that it is possible to prepare flexible transparent conductive films from PVP-coated Pd nanowires by modifying their surfaces with Ag using the deposition method developed in this work. As shown in Fig. 6c, the method reported in this work allowed to easily deposit uniform Ag onto Pd nanowires dispersed in aqueous solutions.

To fabricate uniform Pd nanowire-based transparent conductive films, Pd nanowires with diameter of 10 nm were first prepared using the method developed in our previous study.[24] After washing for several times, the Pd nanowires were dispersed in ethanol and sonicated for 30–60 s. Then the Pd nanowires were consequently deposited on a 140 μm-thick polyethylene terephthalate (PET) substrate by a spin coating technique. After drying under an infrared lamp, the film was transferred into a tube furnace and heated at 130 °C in 5% H_2/N_2 to anneal the Pd nanowires. The deposition of Ag on the Pd nanowires was easily realized by simply mixing the Pd nanowires with aqueous solution of Ag^+ in the presence of H_2 at room temperature. The obtained film was denoted as Pd NWs film@Ag. For comparison, the pre-prepared Pd@Ag nanowires were also employed as the materials to fabricate the film (denoted as Pd@Ag NWs film) by depositing them on PET *via* spin coating (Fig. S8†).

As shown in Fig. 7a and b, the morphology of Pd-based nanowires deposited on PET was not changed after modifying their surface with Ag. The inset of Fig. 7c shows a photograph of the as-prepared Pd NWs film@Ag. The background is clearly seen through the Pd NWs@Ag film, indicating that the film is transparent. The transmittances of the films made of Pd NWs film@Ag, Pd@Ag NWs film and Pd NWs film were nearly constant in both the visible and near-infrared region with average transmittances of ~90.5, ~94.0 and ~96.1% from 400 to 1700 nm, respectively (Fig. 7c). Surprisingly, the Pd NWs film@Ag exhibited much better sheet electronic conductivity (271 S sq^{-1}) than those of Pd NWs film (25 534 S sq^{-1}) and Pd@Ag

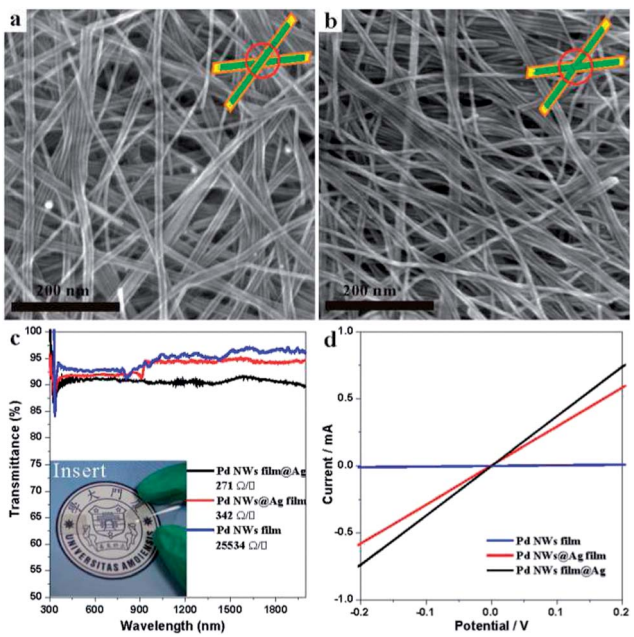

Fig. 7 SEM images of Pd NWs@Ag (a) and Pd NWs film@Ag (b). Insets in (a) and (b) show the different contact structure of nanowires in both samples. (c) Optical transmittance of Pd NW film@Ag, Pd wire@Ag film and Pd NWs films measured with a UV-Vis spectrometer by subtracting the background of PET. (d) Current–voltage curves of the as-made transparent films.

NWs film (342 S sq^{-1}) (Fig. 7d). The better conductivity of Pd NWs film@Ag than the Pd@Ag NWs film suggested that the post Ag deposition process helped to improve the ohmic contacts between Pd@Ag NWs which hindered charge transport. Moreover, the obtained Pd NWs film@Ag was transparent over a wide range of wavelengths.

4 Conclusions

In summary, we have developed a facile method to fabricate core–shell bimetallic Pd@Ag NCs by using Pd NCs as seeds. In the method, gaseous hydrogen was activated on the Pd surface and functioned as the reducing agent for reductive deposition of Ag on Pd. As the reduction agent was generated and confined on the surface of Pd, self-nucleation of Ag was effectively avoided. Mechanism studies demonstrated that the deposition of Ag(0) was accompanied by increase of proton concentrations and self-terminated when the Pd surface was fully covered by Ag. The ratio of Ag/Pd in the resulting Pd@Ag NCs was tunable by either the amount of $AgNO_3$ or H_2. Moreover, the developed deposition method was morphology-independent. Core–shell Pd@Ag nanosheets, nanocubes, tetrahedra and nanowires were successfully synthesized *via* the method. When applied to depositing Ag on pre-fabricated flexible thin-film of Pd nanowires on PET substrate, the method helped improve ohmic contacts between nanowires and thus significantly enhanced their electronic conductivity. Besides Pd nanostructures, the developed method is expected to be effective for preparing other bimetallic nanostructures with metal cores that can activate gaseous H_2 for reductive deposition of shell metals.

Acknowledgements

We thank the MOST of China (2011CB932403, 2014CB932004) and the NSFC of China (21131005, 21333008) for financial support.

References

1 B. Lim, H. Kobayashi, T. Yu, J. Wang, M. J. Kim, Z. Y. Li, M. Rycenga and Y. Xia, *J. Am. Chem. Soc.*, 2010, **132**, 2506–2507.
2 X. Huang, S. Tang, B. Liu, B. Ren and N. Zheng, *Adv. Mater.*, 2011, **23**, 3420–3425.
3 J. Yang, J. Yang and J. Ying, *ACS Nano*, 2012, **6**, 9373–9382.
4 J. Qiu, Y. Wu, Y. Wang, M. Engelhard, L. McElwee-White and D. W. Wei, *J. Am. Chem. Soc.*, 2012, **135**, 38–41.
5 A. Yin, X. Min, Y. Zhang and C. Yan, *J. Am. Chem. Soc.*, 2011, **133**, 3816–3819.
6 H. Zhang, M. Jin, H. Liu, J. Wang, M. J. Kim, D. Yang, Z. Xie, J. Liu and Y. Xia, *ACS Nano*, 2011, **5**, 8212–8222.
7 B. Wu and N. Zheng, *Nano Today*, 2013, **8**, 168–197.
8 A. K. Sra and R. E. Schaak, *J. Am. Chem. Soc.*, 2004, **126**, 6667–6672.
9 Y. Sun, B. T. Mayers and Y. Xia, *Nano Lett.*, 2002, **2**, 481–485.
10 Y. Yu, Q. Zhang, J. Xie and J. Y. Lee, *Nat. Commun.*, 2013, **4**, 1454.
11 M. Chen, J. Kim, J. P. Liu, H. Fan and S. Sun, *J. Am. Chem. Soc.*, 2006, **128**, 7132–7133.
12 S. Sun, C. B. Murray, D. Weller, L. Folks and A. Moser, *Science*, 2000, **287**, 1989–1992.
13 C. Wang, W. Tian, Y. Ding, Y. Ma, Z. L. Wang, N. M. Markovic, V. R. Stamenkovic, H. Daimon and S. Sun, *J. Am. Chem. Soc.*, 2010, **132**, 6524–6529.
14 C. Yang, K. Chanda, P. Lin, Y. Wang, C. Liao and M. H. Huang, *J. Am. Chem. Soc.*, 2011, **133**, 19993–20000.
15 J. Zeng, C. Zhu, J. Tao, M. Jin, H. Zhang, Z. Li, Y. Zhu and Y. Xia, *Angew. Chem., Int. Ed.*, 2012, **51**, 2354–2358.
16 D. Wang and Y. Li, *J. Am. Chem. Soc.*, 2010, **132**, 6280–6281.
17 H. Kobayashi, M. Yamauchi, H. Kitagawa, Y. Kubota, K. Kato and M. Takata, *J. Am. Chem. Soc.*, 2008, **130**, 1828–1829.
18 M. Yamauchi, R. Ikeda, H. Kitagawa and M. Takata, *J. Phys. Chem. C*, 2008, **112**, 3294–3299.
19 F. Taufany, C. Pan, J. Rick, H. Chou, M. Tsai, B. Hwang, D. Liu, J. Lee, M. Tang, Y. Lee and C. Chen, *ACS Nano*, 2011, **5**, 9370–9381.
20 R. M. Anderson, L. Zhang, J. A. Loussaert, A. I. Frenkel, G. Henkelman and R. M. Crooks, *ACS Nano*, 2013, **7**, 9345–9353.
21 X. Huang, S. Tang, X. Mu, Y. Dai, G. Chen, Z. Zhou, F. Ruan, Z. Yang and N. Zheng, *Nat. Nanotechnol.*, 2011, **6**, 28–32.
22 X. Huang, H. Zhang, C. Guo, Z. Zhou and N. Zheng, *Angew. Chem., Int. Ed.*, 2009, **121**, 4902–4906.
23 Y. Dai, X. Mu, Y. Tan, K. Lin, Z. Yang, N. Zheng and G. Fu, *J. Am. Chem. Soc.*, 2012, **134**, 7073–7080.
24 X. Huang and N. Zheng, *J. Am. Chem. Soc.*, 2009, **131**, 4602–4603.
25 T. B. Flanagan and W. A. Oates, *Annu. Rev. Mater. Sci.*, 1991, **21**, 269–304.
26 R. C. Wolfe, K. G. Weil, B. A. Shaw and H. W. Pickering, *J. Electrochem. Soc.*, 2005, **152**, B82–B88.
27 J. H. He, L. F. Dechiaro, D. L. Knies, G. K. Hubler, K. S. Grabowski, A. E. Moser, D. D. Dominguez, D. A. Kidwell and P. L. Hagelstein, *Int. J. Hydrogen Energy*, 2012, **37**, 12351–12357.
28 C. Langhammer, V. P. Zhdanov, I. Zorić and B. Kasemo, *Phys. Rev. Lett.*, 2010, **104**, 135502.
29 F. Yang, D. K. Taggart and R. M. Penner, *Nano Lett.*, 2009, **9**, 2177–2182.
30 F. Yang, S. Kung, M. Cheng, J. C. Hemminger and R. M. Penner, *ACS Nano*, 2010, **4**, 5233–5244.
31 L. Hu, H. S. Kim, J. Lee, P. Peumans and Y. Cui, *ACS Nano*, 2010, **4**, 2955–2963.
32 M. Hu, J. Gao, Y. Dong, K. Li, G. Shan, S. Yang and R. K. Y. Li, *Langmuir*, 2012, **28**, 7101–7106.
33 J. Lee, S. T. Connor, Y. Cui and P. Peumans, *Nano Lett.*, 2008, **8**, 689–692.

